Second order optical nonlinearity in silicon waveguides - inhomogeneous stress and interfaces

Clemens Schriever[1]*, Federica Bianco[2†]*, Massimo Cazzanelli[2], Mher Ghulinyan[3], Christian Eisenschmidt[4], Georg Schmidt[4], Johannes de Boor[5],Alexander Schmid[6], Johannes Heitmann[6], Lorenzo Pavesi[2], Jörg Schilling[1]

[1]*Centre for Innovation Competence SiLi-nano, Martin-Luther-University Halle-Wittenberg, Karl-Freiherr-von-Fritsch-Str. 3, 06120 Halle (Saale), Germany*

[2]*Nanoscience Laboratory, Department of Physics, University of Trento, via Sommarive 14, 38123 Povo, Trento, Italy*

[3]*Advanced Photonics & Photovoltaics Unit, Bruno Kessler Foundation, via Sommarive 18, 38123 Povo, Trento, Italy*

[4]*Institute of Physics, Martin-Luther-University of Halle-Wittenberg, Heinrich-Damerow-Str. 4, 06120 Halle (Saale), Germany*

[5]*Max Planck Institute of Microstructure Physics, Weinberg 2, 06120 Halle (Saale), Germany*

[6]*Institut für Angewandte Physik, TU Bergakademie Freiberg, Leipziger Str. 23, 09599 Freiberg, Germany and*

[†]*present address: NEST, Istituto Nanoscienze-CNR and Scuola Normale Superiore, P.za S. Silvestro 12, 56127 Pisa, Italy*

**Both authors have contributed equally to this work.*

(Dated: October 28, 2013)

The lack of a dipolar second order susceptibility ($\chi^{(2)}$) in silicon due to the centrosymmetry of its diamond lattice usually inhibits efficient second order nonlinear optical processes in the silicon bulk. Recently the deposition of stressed silicon nitride layers and the corresponding inhomogeneous strain in silicon lead to the demonstration of second harmonic generation and electro-optic modulation in strained silicon waveguides. However, the respective impact of the stress/strain gradient and the involved interfaces was not clear. Here, we investigate the influence of the stress and the stressing silicon nitride layer using second harmonic generation measurements in transmission. The results show, that the enhancement of the second order nonlinearity arises from a constructive superposition of stress-induced and interface-related effects. Particularly, the stress gradient in silicon breaks the symmetry of the crystal lattice, while positive fixed charges at the silicon/silicon nitride interface are responsible for a pronounced electric-field-induced-second harmonic (EFISH) contribution. These results demonstrate the impact of external factors for the creation of an effective ($\chi^{(2)}$) in materials and open new perspectives for the use of second order nonlinear optical processes in silicon photonics.

Although silicon photonics obtained an established technology basis in the last years, nonlinear optical processes like difference frequency generation or ultrafast electro-optic modulation using the linear electrooptic effect are not possible in silicon. On a fundamental level this is caused by the centrosymmetry of the silicon crystal lattice, which results in a lack of a dipolar bulk ($\chi^{(2)}$). Therefore, nonlinear active devices based on silicon are usually fabricated by exploiting its third order nonlinearity ($\chi^{(3)}$) [1] or combining various nonlinear materials with silicon [2–4]. However, since silicon exhibits a strong two-photon absorption in the near infrared, the efficiency of these processes is limited. Therefore researcher tried to breack the centrosymmetry of bulk silicon crystal deliberately to induce a non zero $\chi^{(2)}$ by using a free surface or an interface [5–8] or by deforming the silicon lattice through a stressing layer [9–11]. Recently, the stressing layer method was used to demonstrate second harmonic generation (SHG) [12] and electro-optical modulation [13, 14] in strained silicon waveguides. In both cases a silicon nitride (SiN_x) overlayer was used to induce the stress inside the silicon waveguide core. However since some authors claim that a second order nonlinearity was observed from silicon nitride itself [15–19], the different impact of interface, stress and nature of the overlayer on the second order nonlinearity is not clarified yet.

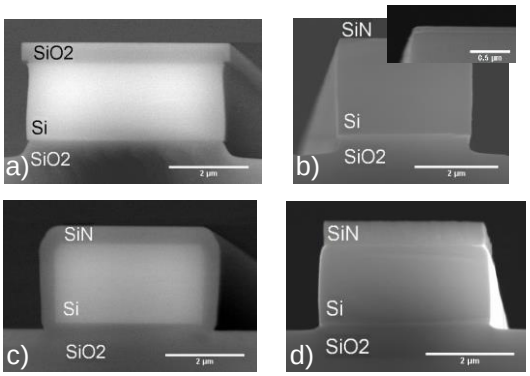

FIG. 1. Reflection Electron Microscopy (REM) images of the investigated waveguides facets. a) 500 nm SiO_2 covered, named SiO2, b) 50 nm SiN_x layer, named SiN2, c) 500 nm SiN_x completely coated, named SiN4, d) 500 nm SiN top coated, named SiN1

In this Letter, we investigate the influence of the stress and the existance of a silicon nitride overlayer on the second order nonlinear response of strained silicon waveguides. We will show a direct correlation of the integrated stress gradient in the silicon lattice (which is a measure of the breaking of the centrosymmetry of the Si-lattice)

TABLE I. Parameters of the samples investigated here. The reported stress values were obtained by wafer bow measurement on complete wafers coated under identical conditions as the respective samples. Negative stress values describe compressively stressed layer resulting in tensile stress in the silicon and vice versa.

Sample	SiRef	SiO2	SiN0	SiN1	SiN2	SiN3	SiN4
Layer	-	top	compl.	top	top	top	compl.
Thk. [nm]	-	500	50	500	50	150	500
Layer-stress [MPa]	-	-300	-7	+ 226	- 880	+1250	+226

with the conversion efficiency for second harmonic generation. In addition we discuss the impact of the silicon nitride cover layers and specifically of their interface with Si. For this purpose a set of silicon-on-insulator waveguide samples was investigated under various conditions of mechanical stress. An overview of the different sample structures is given in Fig. 1 and Tab. I. The set consists of a reference sample SiRef with uncoated 2 µm thick Si strip waveguides resting on a buried oxide layer with the same thickness. Furthermore, a sample SiO2 (Fig. 1 a)), whose waveguides were covered with a layer of stressing thermal oxide, was produced. A comparison of the second harmonic (SH) conversion efficiencies of both samples can be used to study the impact of the stress on the second order nonlinearity. Additionally, samples with different silicon nitride overlayers were produced. Sample SiN0 was completely covered with a thin almost unstressed SiN_x overlayer to investigate the influence of the SiN_x layer alone, excluding any stress related effects. To examine the combination of SiN_x and stress effect, additional silicon nitride samples were processed with different stress extent, stress sign and layer thicknesses. Except for sample SiN3, which was covered using low pressure chemical vapor deposition (LPCVD), all nitride covered samples were coated using the plasma enhanced chemical vapor deposition (PECVD) technique. Here, the method of dual frequency deposition was used to vary the stress in the deposited layer without changing the composition of the plasma [20].

To relate the second order response measured in the nonlinear transmission experiments with the stress state of the waveguides, a finite element method (FEM) model was employed to estimate the stress tensor across the waveguide cross section, where a plane stress regime was assumed [21, 22]. Fig. 2 shows the distribution of the normal stress component σ_{xx} and the local stress gradient (arrows) for 10 µm wide waveguides of different samples. Moreover, based on the sp^3 orbital models [9, 10], a linear relationship between the second order susceptibility $\chi^{(2)}$ and the stress gradient was assumed. A rigourous analysis would require the study of the influence of the local stress gradient on the local nonlinear optical properties of the waveguide core. However, the measurements

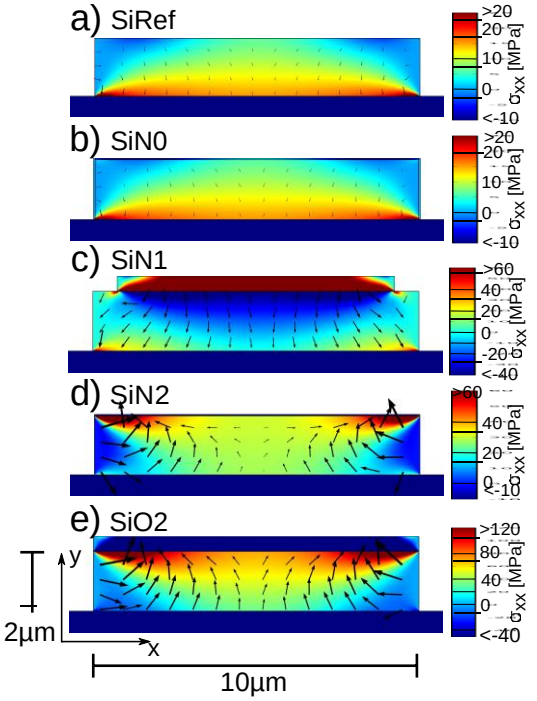

FIG. 2. Simulated distribution of the stress component σ_{xx} along the cross section of 10 μm wide waveguides for sample SiRef a), SiN0 b) SiN1 c), SiN2 d) and SiO2 e), as well as the resulting stress gradient (arrows).

of the second harmonic light in transmission represent a non-simple average of the local contributions along the waveguide cross section. Therefore, a total stress gradient was used to describe the overall stress inhomogeneity in the various samples. This was quantified by integrating the sum of the local gradients of the stress tensor components over the waveguide cross section as follows

$$\Sigma = \int \left| \frac{d\sigma_{xx}}{dx} \right| + \left| \frac{d\sigma_{xx}}{dy} \right| + \left| \frac{d\sigma_{yy}}{dx} \right| + \left| \frac{d\sigma_{yy}}{dy} \right| + \left| \frac{d\sigma_{xy}}{dx} \right| + \left| \frac{d\sigma_{xy}}{dy} \right| dA, \quad (1)$$

A comparison of the stress distribution in the samples SiRef and SiN0 (Fig. 2 a) and b)) shows that the thin SiN_x cover layer has no influence on the stress inside the waveguide. On the contrary, the stress distribution is slightly affected by the stress in the underlying oxide layer that is created during the fabrication of the SOI wafer (Σ_{SiRef} = 436 N/m, Σ_{SiN0} = 383 N/m) [12, 23]. A stronger influence on the stress can be seen for the samples SiN1 and SiN2 with a stressed SiN_x layer on top (Fig. 2 c) and d)). Both samples show almost the same Σ (Σ_{SiN1} = 1535 N/m, Σ_{SiN2} = 1559 N/m). However, as both samples are coated with layers of different thickness and stress level, the local stress gradients differ strongly from each other. In Fig. 2 e) the stress distribution in the SiO_2 coated sample is shown, exhibiting a strong

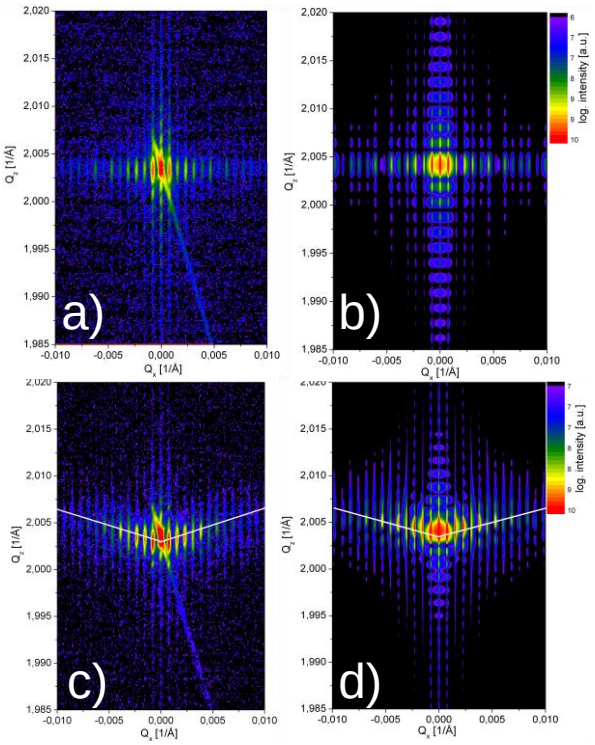

FIG. 3. Comparison between experimentally (left) and numerically (right) determined RSM. In case of a stressing layer the diffracted intensity shifts to higher Q_z values (white line). The additional feature in a) and c) represents the analyzer streak related to the x-ray setup. The strong agreement of the RSM proves the accuracy of the FEM model used for the calculations.

total stress gradient of Σ_{SiO_2} = 3197 N/m.

To test the reliability of the employed FEM model for the calculation of the stress gradients, the stress distribution in a reference system has been modeled. The system consists of (111) oriented, laser written [24] silicon grating structures, stressed by a 110 nm thermal SiO_2-layer (σ = -450 MPa). The numerical results were used to calculate artificial reciprocal space maps (RSM), that were compared to experimental ones determined by high resolution x-ray diffraction (HRXRD) for the (111)-reflex. In comparison to the diffraction pattern of the unstrained grating (Fig. 3 a)), the strained grating exhibits to bending of its diffraction pattern in Q_z direction (Fig. 3 c)). The artificial RSMs were calculated using kinematic diffraction theory [25]. By this means the amplitude of the field scattered by a single ridge can be expressed as [26]

$$A_{tooth} = \sum_i F \exp\left(i\vec{Q}\,(\vec{r}_i + \vec{u}(\vec{r}_i))\right). \qquad (2)$$

The ridge is split into identical unit cells (10 × 10 atoms) with a form-factor F located at the position $\vec{r}_i + \vec{u}(\vec{r}_i)$. Here $\vec{r}_i$ describes the position of the cell in the unstressed case while $\vec{u}(\vec{r}_i)$ represents the additional displacement of

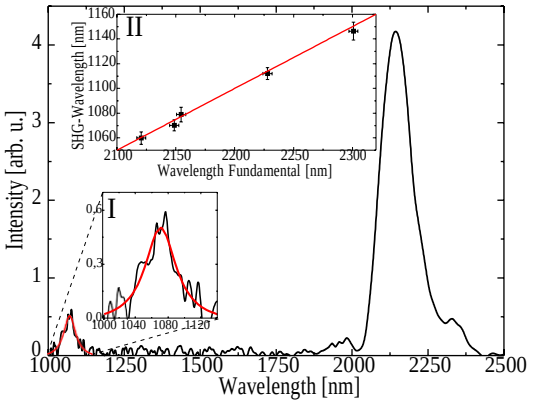

FIG. 4. SHG measurements of a 10 μm wide waveguide of sample SiO2 showing peaks at the fundamental (λ_ω = 2.14 μm) and SH wavelengths ($\lambda_{2\omega}$ = 1.07 μm). The coupled average power of the fundamental beam was about 0.15 μW. Inset I shows the zoom of SH peak, where the red line is the fitting Gaussian curve. Inset II shows the wavelength tunability of the SH signal. The red line is the expected relationship between $\lambda_{2\omega}$ and λ_ω.

the respective cell due to the local strain. The data for the position of the displaced unit cells was taken from the FEM model that was calculated using the actual parameters of the sample. For the artificial RSM the contribution of several ridges was taken into account by summing over the contribution of N single ridge separated by a lattice constant Γ:

$$A_{total} = A_{tooth} \cdot \left(1 + e^{iQ_x\Gamma} + \cdots + e^{iQ_xN\Gamma}\right) = A_{tooth} \cdot \frac{e^{iQ_x\Gamma(N+1)} - 1}{e^{iQ_x\Gamma N} - 1}. \qquad (3)$$

A comparison between the experimentally determined and calculated RSM (Fig.3 a, c) and Fig.3 b, d), respectively) shows a good agreement for both cases - the stressed and unstressed geometries. This result proves that the FEM model is suitable to represent the actual stress distribution inside a stressed silicon waveguide and that the calculated inegrated stress gradient discussed above is reliable .

To investigate the second order nonlinear optical properties of the different samples, the SH signal from 2 mm long waveguides was measured in transmission using a tunable laser source with 100 fs-pulses at a wavelength of about 2200 nm. The coupling of the pump light in and out of the waveguides was accomplished by gold coated reflecting mirror objectives. By imaging the transmitted beam onto an IR Vidicon Camera, the best waveguide coupling was assured. The signal from the waveguide was also recorded by a Fourier transform infrared spectrometer (FTIR) equipped with a LN_2-cooled InSb-detector, which allowed simultaneous recording of the signal at fundamental and SH wavelengths (Fig. 4). For one spectrum an average of over 1000 single measurements was taken.

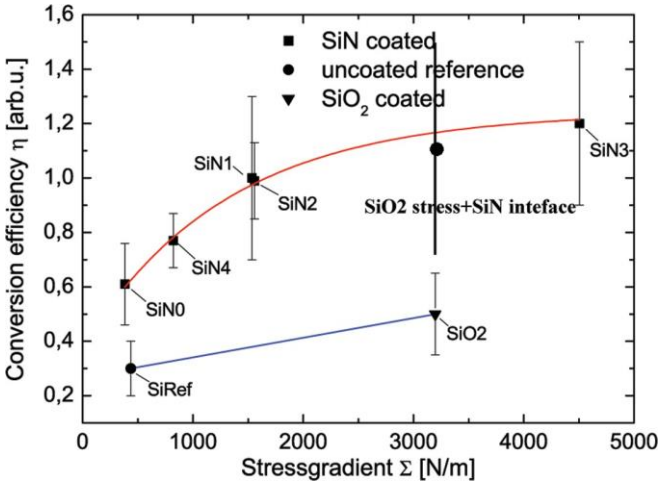

FIG. 5. Dependence of the experimentally determined nonlinear conversion efficiency η on the total stress gradient Σ for 10 μm wide waveguides under different stressing conditions. The lines are guides to the eye.

To reduce the error when estimating the intensity of the SH peak, a Gaussian curve was fitted to the spectrum (Fig. 4 Inset I). Inset II shows the typical linear dependence between the wavelengths of the second harmonic and fundamental beams for a SHG process.

As it was not possible to estimate the exact SH intensity, no absolute $\chi^{(2)}$ values could be calculated. Instead, a relative conversion efficiency η was determined, which allows a comparison of the second order nonlinearities of the different samples measured under identical conditions. As the conversion efficiency was expected to be rather low, the effect of pump depletion was neglected here. The conversion efficiency was defined as:

$$\eta = \frac{I_{2\omega}}{I_{\omega}^2} \qquad (4)$$

that is the ratio between the SH intensity ($I_{2\omega}$) and the squared excitation intensity (I_{ω}).

Figure 5 relates the estimated conversion efficiency η to the calculated total stress gradient Σ. To ensure confidence in the obtained values, η has been evaluated from at least three different waveguides with identical parameters. The error bars result from the maximum semi-dispersion of the determined values. For sample SiRef only a weak SH signal was generated.It is caused by contributions from the waveguide surfaces and the interface between silicon and native and buried SiO_2 layers, where the centrosymmetry is locally broken. A clear increase of η was observed in the stressed SiO_2 covered sample (SiO2) (Fig. 5). In this sample the interface contributions can be considered comparable to the ones of sample SiRef, since also SiRef carries a natural oxide layer of a few nm thickness. Instead, analyzing the mechanical states of the two samples (Σ_{SiRef} = 436 N/m and Σ_{SiO_2} = 3197 N/m), the sample SiO2 shows a much larger total stress gradient, that indicates a stronger deformation of the Si-Si bonds in the crystalline lattice. The enhancement observed in the conversion efficiency can be thus attributed to the effect of the inhomogeneous stress inside the waveguide core, that agrees with earlier statements [12].

When studying the conversion efficiency of the samples coated with a stressing silicon nitride layer (Fig. 5), it can be seen that η increases when the stress gradient increases. This is particularly obvious for the strongly stressed SiN2 sample. It has the same film thickness, but a very different stress level compared to the quasi unstressed SiN0 sample. This confirms the existence of the stress related effect on $\chi^{(2)}$ also in the SiN_x-stressed samples.

To examine a possible nonlinear effect due to the SiN_x layer itself, the conversion efficiencies of SiRef and the silicon nitride covered (but quasi unstressed) sample SiN0 were compared. For SiN0 the conversion efficiency η is enhanced by a factor of approximately two compared to SiRef. This indicates an unexpectedly strong influence of the silicon nitride layer or its interface. In addition one notes, that this contribution adds constructively to the stress effect, leading to an overall stronger enhancement of the effective nonlinearity than in the case of sample SIO2. Additional support for the superposition of both effects (stress related and SiN_x-related) is gained by adding the SiN_x layer contribution from sample SiN0 to the conversion efficiency measured in sample SIO2. Interestingly, the resulting η value appears aligned with the trend observed for the other stressed SiN_x covered samples (diamond marker in Fig. 5).

The origin of the strong SH signal in the quasi unstressed sample SiN0 is indeed puzzling. From the presented results, we conclude that the reason for its increased SH-intensity has to lie within the SiN_x layer or the SiN_x/Si-interface. However results and interpretations from literature are not conclusive in this respect. Previous studies on second order nonlinearity in silicon nitride reported the observation of a strong SHG from PECVD silicon nitride films grown on fused silicon oxide substrate [16], where the nonlinearity was assigned to a SiN_x bulk origin. On the other hand, an interface-induced $\chi^{(2)}$ was reported in thin film Bragg reflectors fabricated in various compositions of amorphous silicon nitride [17], in high-quality amorphous silicon nitride (a-$Si_{1-x}N_x$:H) Fabry-Perot microcavities [18] and in multilayer silicon-oxy-nitride (SiON) waveguides [19]. Furthermore, a SH signal was generated in PECVD silicon nitride ring resonators [15], where the nonlinearity was attributed to the interface between the silicon nitride and the silicon oxide. In our case, the high index contrast in the present waveguides implies a strong confinement of the guided mode to the silicon core, which may exclude a deeper penetration of the mode into the silicon nitride

layer. Thus a contribution from a however possible silicon nitride bulk $\chi^{(2)}$ seems negligible in our case.

To then clarify the impact of the SiN_x/Si-interface we investigated the charge state of the SiN_x layers. Capacitance-Voltage (C-V) measurements were carried out at SiN_x-layers which were deposited in the same way as the samples SiN0 and SiN1 (see supplementary information). For both cases a very similar fixed areal charge density of $\sigma_{fix} = 1.5 \cdot 10^{12}cm^{-2}$ and $\sigma_{fix} = 1.2 \cdot 10^{12}cm^{-2}$ was found for the SiN_x-layers. Since the thickness of the SiN_x-layers has no impact on the absolute charge of the layers, we conclude that the observed positive fixed charges are located within a very thin sheet close to the Si/SiN_x-interface. For the given charge densities electric fields of $2.3 \cdot 10^5$V/cm and $1.8 \cdot 10^5$V/cm at the interface are obtained, respectively [27]. These fields are strong enough to create an inversion layer in the silicon, and although the electric field drops fast in an inversion layer, a sizeable field of the order of 10^4 V/m still penetrates for a few 100 nm into the silicon. In this region the electric field breaks the centrosymmetry of the silicon band structure, so that electric field induced second harmonic generation (EFISH) emerges from there. Consequently, in our waveguides the SiN_x-related enhancement of the SHG in absence of stress can be attributed to the EFISH-effect in the space charge layer close to the Si/SiN_x-interface. Note, that in silicon technology EFISH is a known effect. For example, it was thoroughly investigated at MOS-capacitors [28], where a voltage was applied across the MOS-structure generating electric fields of the order of 10^5 V/cm in the silicon space charge layer. As a result, a manifold enhancement of the SH signal was observed in reflection from the dielectric/semiconductor interface of the MOS-structure.

Moreover, the similarity of the measured fixed charge density of the two samples is also surprising in a different way. Although the deposition regimes for the SiN_x-layers were quite different to obtain the different stress levels, the same charge density was obtained. From this we might conclude that all our investigated SiN_x-layers have the same fixed charge density and with this the same level of EFISH appears in all the SiN_x-coated samples. This further supports our earlier assumption that we can add the same offset in SHG-enhancement to the conversion efficiencies of all SiN_x-covered samples in Fig. 5.

In conclusion, the influences of the inhomogeneous stress and the presence of a silicon nitride layer on the second order nonlinearity in silicon waveguides could be separated. Both schemes enhance the nonlinear optical response of the waveguides. While the stressed layers create an inhomogeneous strain field within the silicon and break its centrosymmetry in this way, the enhancement due to the SiN_x alone was attributed to the fixed positive charges close to the Si/SiN_x-interface, which lead to a strong electric field in the silicon near the interface and cause a pronounced EFISH contribution. It was also found, that both contributions add up constructively, which allows the combination of both methods to further enhance the effective nonlinearity of the waveguides in the future.

C. Schriever and J. Schilling would like to thank the Federal Ministry for Education and Research ("Bundesministerium fur Bildung und Forschung") for their financial support within the Centre for Innovation Competence SiLi-nano (project number 03Z2HN12) and Prof. Ulrich Hilleringmann for providing the PECVD deposition. F. Bianco, M. Cazzanelli, M. Ghulinyan and L. Pavesi would like to thank the Provincia Autonoma di Trento and Fondazione Cariplo for their financial support in the framework of the FUPAT- NAOMI project and by the grant number 2009-2730, respectively.

[1] C. K. J. Leuthold and W. Freude, Nature Photon. **4**, 535 (2010).
[2] C. Koos, L. Jacome, C. Poulton, J. Leuthold, and W. Freude, Opt. Express **15**, 5976 (2007).
[3] C. Koos, P. Vorreau, T. Vallaitis, P. Dumon, W. Bogaerts, R. Baets, B. Esembeson, I. Biaggio, T. Michinobu, F. Diederich, W. Freude, and J. Leuthold, Nat. Photonics **3**, 216 (2009).
[4] C. Schriever, C. Bohley, and J. Schilling, Photonics and Nanostructures - Fundamentals and Applications **10**, 312 (2012).
[5] S. Mitchell, M. Mehendale, D. Villeneuve, and R. Boukherroub, Surface Science **488**, 367 (2001).
[6] J. E. Mejia, B. S. Mendoza, M. Palummo, G. Onida, R. Del Sole, S. Bergfeld, and W. Daum, Phys. Rev. B **66**, 195329 (2002).
[7] J. E. Sipe, D. J. Moss, and H. M. van Driel, Phys. Rev. B **35**, 1129 (1987).
[8] N. Bloembergen, Appl. Phys. B **68**, 289 (1999).
[9] J. Y. Huang, Jpn. J. Appl. Phys. **33**, 3878 (1994).
[10] S. V. Govorkov, V. I. Emel'yanov, N. I. Koroteev, G. I. Petrov, I. L. Shumay, and V. V. Yakovlev, JOSA B **6**, 1117 (1989).
[11] C. Schriever, C. Bohley, and R. B. Wehrspohn, Opt. Lett. **35**, 273 (2010).
[12] M. Cazzanelli, F. Bianco, E. Borga, G. Pucker, M. Ghulinyan, E. Degoli, E. Luppi, V. Véniard, S. Ossicini, D. Modotto, S. Wabnitz, R. Pierobon, and L. Pavesi, Nat. Mater. **11**, 148 (2011).
[13] R. S. Jacobsen, K. N. Andersen, P. I. Borel, J. Fage-Pedersen, L. H. Frandsen, O. Hansen, M. Kristensen, A. V. Lavrinenko, G. Moulin, H. Ou, C. Peucheret, B. Zsigri, and A. Bjarklev, Nature **441**, 199 (2006).
[14] B. Chmielak, M. Waldow, C. Matheisen, C. Ripperda, J. Bolten, T. Wahlbrink, M. Nagel, F. Merget, and H. Kurz, Opt. Express **19**, 17212 (2011).
[15] J. S. Levy, M. A. Foster, A. L. Gaeta, and M. Lipson, Opt. Express **19**, 11415 (2011).
[16] T. Ning, H. Pietarinen, O. Hyvarinen, J. Simonen, G. Genty, and M. Kauranen, Appl. Phys. Lett. **100**, 161902 (2012).
[17] S. Lettieri, S. D. Finizio, P. Maddalena, V. Ballarini, and

F. Giorgis, Appl. Phys. Lett. **81**, 4706 (2002).
[18] E. Descrovi, C. Ricciardi, F. Giorgis, G. Lérondel, S. Blaize, C. X. Pang, R. Bachelot, P. Royer, S. Lettieri, F. Gesuele, P. Maddalena, and M. Liscidini, Opt. Express **15**, 4159 (2007).
[19] D. F. Logan, A. B. A. Dow, D. Stepanov, P. Abolghasem, N. P. Kherani, and A. S. Helmy, Appl. Phys. Lett. **102**, 061106 (2013).
[20] L. Vanzetti, M. Barozzi, D. Giubertoni, C. Kompocholis, A. Bagolini, and P. Bellutti, Surf. Interface Anal. **38**, 723 (2006).
[21] I. D. Wolf, H. E. Maes, and S. K. Jones, Journal of Applied Physics **79**, 7148 (1996).
[22] S. Narayanan, S. R. Kalidindi, and L. S. Schadler, Journal of Applied Physics **82**, 2595 (1997).
[23] F. Bianco, K. Fedus, F. Enrichi, R. Pierobon, M. Cazzanelli, M. Ghulinyan, G. Pucker, and L. Pavesi, Semicond. Sci. Technol. **27**, 085009 (2012).
[24] J. de Boor, N. Geyer, J. V. Wittemann, U. Gösele, and V. Schmidt, Nanotechnology **21**, 095302 (2010).
[25] B. E. Warren, *X-ray Diffraction* (Courier Dover Publications, 1969).
[26] U. Pietsch, V. Holý, and T. Baumbach, *High-Resolution X-Ray Scattering - From Thin Films to Lateral Nanostructures* (Spinger-Verlag, 2004).
[27] O. A. Aktsipetrov, A. A. Fedyanin, A. V. Melnikov, E. D. Mishina, A. N. Rubtsov, M. H. Anderson, P. T. Wilson, M. ter Beek, X. F. Hu, J. I. Dadap, and M. C. Downer, Phys. Rev. B **60**, 8924 (1999).
[28] O. A. Aktsipetrov, A. A. Fedyanin, E. D. Mishina, A. N. Rubtsov, C. W. van Hasselt, M. A. C. Devillers, and T. Rasing, Phys. Rev. B **54**, 1825 (1996).